# A numerical study on free vibration analysis of detailed and homogenized models for FG-CNTRC beams

**Hyeong Jin Kim[1] and Jin-Rae Cho[2]**

[1]Department of Mechanical Engineering, University College London, London, WC1E 7JE, UK, [2] Department of Naval Architecture and Ocean Engineering, Hongik University, Sejong, 30016, Korea

(Received 000 0, 2020; Revised 000 0, 2020; Accepted 000 0, 2020)

Keywords: Functionally graded nanocomposite, Carbon nanotube-reinforced composite (CNTRC) beam, Free vibration, Detailed model, Homogenized model, Finite element analysis

Correspondence to: Jin-Rae Cho / jrcho@hongik.ac.kr

**Abstract** The goal of this study is to compare and investigate the free vibration characteristics of detailed and homogenized models for functionally graded carbon nanotube-reinforced composite (FG-CNTRC) beams, based on the finite element method (FEM). In this study, three types of FG-CNTRC beams and boundary conditions are considered for different volume fractions of CNT: UD (uniformly distributed), FG-X, and FG-Λ beams. These beams in which single-walled carbon nanotubes (SWCNTs) are distributed with a gradient through the thickness are employed and analyzed for simply supported (SS), clamped-clamped (CC), and free-free (FF) boundary conditions. For the homogenized model, the effective material properties are determined in terms of the CNT volume fraction using the linear rule of mixture. A commercial midas NFX program is used for finite element simulations to analyze the free vibration responses of FG-CNTRC beams. The numerical results are compared with the existing analytical solutions in the literature in order to validate the developed finite element models.

## 1. Introduction

Carbon nanotube (CNT) is receiving considerable attention as an innovative filler that outperforms the conventionally used composite materials, owing to its excellent physical, mechanical, and thermal characteristics. CNT-reinforced composite materials are used in nanomaterial processing technology in various industries such as automobile, architecture, aerospace, marine, and electrical/electronics, thereby increasing productivity.

The vibration characteristics of structural members such as beams, plates and shells must be evaluated for safety diagnosis and accident prevention [1]. However, materials and vibration properties tend to change even if CNT of the same weight is inserted because the matrix and CNT volume fraction distribution can change in a functionally graded carbon nanotube-reinforced composite (FG-CNTRC). Hence, various studies have focused on theoretical and numerical investigation of the free vibration characteristics of the FG-CNTRC beam. Reddy [2] performed natural vibration analysis on the FG-CNTRC beam using the modified couple stress theory and compared the results with those obtained using conventional beam theory. Yas and Samadi [3] analyzed the natural vibration of the elastic foundation-based FG-CNTRC Timoshenko beam and examined the effect of the CNT volume fraction distribution on the natural frequency of the beam. Shenas et al. [4] analyzed the natural vibration of the FG-CNTRC beam with initial torsion under various temperature conditions and torsion angles using the Chebyshev–Ritz technique. The results indicated that the temperature increases with a decrease in the natural frequency, and the twist angle increases with the natural frequency.

Duc et al. [5-6] investigated the nonlinear dynamic response and free vibration of imperfect FG-CNTRC double curved shallow shells and analyzed the free vibration of cracked FG-CNTRC plates using phase filed theory. Thanh et al. [7] presented the vibration and nonlinear dynamic response of imperfect FG-CNTRC plates on elastic foundations subject to dynamic loads and temperature. Karamanli and Vo [8] performed the natural vibration analysis on the FG-CNTRC beam applying the finite element method to shear deformation theory and demonstrated that the volume fraction increases with natural frequency. Dat et al. [9] investigate the influence of the major parameters on the vibration and nonlinear dynamic analysis of sandwich FG-CNTRC plate with porous core layer. Cho [10] investigated the free vibration of FG-CNTRC sandwich plates with a homogeneous core.

The size effect can cause a significant error unless nanoscopic materials, including CNT, are analyzed at a microscopic level, even in molecular dynamics [11]. However, because the nanoscopic analysis method has limitations in practice, such as high computation time, a homogenization method is used as an

improved alternative. Numerous studies have investigated the free vibration characteristics of the CNTRC beam, plate, and panel using the homogenization technique. However, these studies are limited to analysis methods that investigate the differences by comparing boundary conditions and types of functional gradients or by applying multi-scale techniques. Hence, studies focusing on the differences in the vibration characteristics obtained using the detailed and homogenized models considering the structural parameters of CNT remain limited.

This study examines the differences in free vibration behavior between the detailed and homogenized models based on the CNT volume fraction and boundary conditions of the FG-CNTRC beam. The results are compared with the analytical solutions reported in previous studies to verify the reliability of the numerical analysis. The analysis considers the differences between the detailed and homogenized models as well as the effects of volume fraction and boundary condition on the natural frequency change.

## 2. FG-CNTRC Beam

FG-CNTRC is a composite material obtained by applying the concept of the conventional functionally graded material (FGM) to CNT. Research on the mechanical properties of FG-CNTRC is being actively conducted, and various types of FG-CNTRC have been introduced, in which the material and the vibration property of the FG-CNTRC beam considerably vary depending on the volume fraction and distribution of CNT. This study considers three types of FG-CNTRC beams (UD, FG-X, and FG-Λ) with polymethyl methacrylate (PMMA) and SWCNT (10,10) used for the matrix and CNT, respectively, as shown in Fig. 1. Tables 1 and 2 list the properties of these materials and the CNT efficiency parameters $\eta_j$ ($j$ = 1, 2, 3) according to the volume fraction. Material properties were calculated numerically via molecular dynamics (MD) simulation, and the efficiency parameters were calculated using a mixture rule based on MD simulation results [12].

The volume fraction $V_{CNT}^{*}$ occupied by CNT in the FG-CNTRC beam was calculated using Eq. (1), and three-total volume fractions ($V_{CNT}^{*}$ = 0.12, 0.17, and 0.28) were considered. The CNT distribution in the thickness direction is shown in Fig. 1 (b) and the corresponding CNT volume fraction can be mathematically expressed using Eq. (2). Here, the FG-CNTRC beam with the same volume fraction carries the same size and number of inserted CNTs.

$$V_{CNT}^{*}=\frac{m_{CNT}}{m_{CNT}+\frac{\rho_{CNT}}{\rho_M}-\frac{\rho_{CNT}}{\rho_M}m_{CNT}} \tag{1}$$

$$\begin{cases} V_{CNT}(z)=V_{CNT}^{*} & \text{(UD)} \\ V_{CNT}(z)=2\left(\dfrac{2|z|}{h}\right)V_{CNT}^{*} & \text{(FG-X)} \\ V_{CNT}(z)=\left(1-\dfrac{2z}{h}\right)V_{CNT}^{*} & \text{(FG-}\Lambda\text{)} \end{cases}, \tag{2}$$

The subscripts CNT and M represent the CNT and matrix, respectively; $V_{CNT}^{*}$ and $V_{CNT}(z)$ are the CNT volume fraction and volume fraction distribution, respectively; $m_{CNT}$ is the mass fraction of CNT; $\rho_{CNT}$ and $\rho_M$ are the densities of CNT and matrix, respectively.

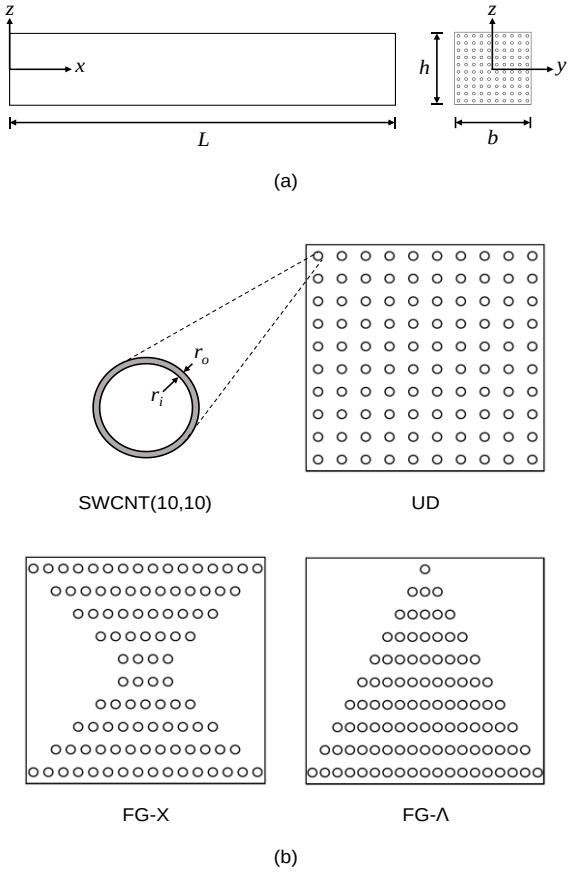


Fig. 1. FG-CNTRC beam: (a) coordinate system and dimensions; (b) cross section of SWCNT(10,10), UD, FG-X, and FG-Λ.

Table 1. The material properties of PMMA and SWCNT.

| | $E_{11}$ [GPa] | $E_{22}$ [GPa] | $G_{12}$ [GPa] | $\nu_{12}$ | $\rho$ [kg/m$^3$] |
|---|---|---|---|---|---|
| PMMA | 2.5 | 2.5 | 0.9 | 0.340 | 1150 |
| SWCNT | 5646.6 | 7080.0 | 1944.5 | 0.175 | 1400 |

Table 2. The efficiency parameters $\eta_j$ ($j$=1,2,3) for different volume fractions $V_{CNT}^{*}$ of CNT.

| $V_{CNT}^{*}$ | $\eta_1$ | $\eta_2$ | $\eta_3$ |
|---|---|---|---|
| 0.12 | 0.137 | 1.022 | 0.715 |
| 0.17 | 0.142 | 1.626 | 1.138 |
| 0.28 | 0.141 | 1.585 | 1.109 |

### 2.1 Detailed Model

The FG-CNTRC beam used for the detailed model in the finite element analysis (FEA) is based on 3-D elasticity theory has the width $b$ and the height $h$ of 10 mm. The length $L$ of the beam was changed to 100 and 250 mm according to the analytical reference solution conditions presented in Section 4. As discussed previously, the microscopic analysis techniques such as the molecular dynamics should be performed for the precise analysis of nanocomposites. However, CNTs are modeled in millimeters (mm) instead of nanometers (nm) for convenience of analysis as the objective of this study is to compare the differences between the detailed and homogenized models.

The CNT used in FEA is assumed to be SWCNT (10,10) in the form of a thin cylinder with a single wall. The CNT outer diameter $r_o$ and inner diameter $r_i$ are calculated using the area ratio considering the volume fraction and the efficiency parameters of CNTs, as expressed in Eq. (3). The area ratio inserted one CNT per cross-section of a 1 mm × 1 mm matrix, and a indicates the width of the matrix used to calculate the area ratio. The outer and inner diameters of the CNT finite element model, calculated using Eq. (3), increase in proportion to the total volume fraction of CNT as listed in Table 3.

$$r_o = \sqrt{\frac{V_{CNT}^*}{\pi}}a, \quad r_i = \sqrt{1-\eta_1}r_o \tag{3}$$

Table 3. The computed outer and inner diameters with respect to the volume fraction $V_{CNT}^*$.

| $V_{CNT}^*$ | $r_o$ (mm) | $r_i$ (mm) |
|---|---|---|
| 0.12 | 0.1954 | 0.1816 |
| 0.17 | 0.2326 | 0.2155 |
| 0.28 | 0.2985 | 0.2767 |

### 2.2 Homogenized Model

The homogenized model offers the computational efficiency than the detailed model since CNTs with the extremely small diameter are replaced with a homogenized matrix. The detailed modelling of CNTs is not only painstaking but also generates a huge number of finite elements, which in turn requires relatively long CPU time. The homogenization technique is an effective method that predicts the thermo-mechanical behavior of materials by approximating the effective material properties of dual-phase nanocomposites such as CNTRC. Typically, the linear rule of mixture [13-14], Mori-Tanaka's mean field theory [15], the self-consistent method [16], and the unit-cell model [17] are widely used. In this study, the linear rule of mixture is used to construct the homogenized model, as it is relatively simple to calculate and yields highly accurate results in the case of simple structures. Eqs. (4) to (8) are used in the calculation, wherein $E$ denotes the Young's modulus, $G$ the shear modulus, and $v$ the Poisson's ratio. Fig. 2 shows the change in effective material property in the thickness direction of the homogenized model calculated with the volume fraction $V_{CNT}^*$ of 0.17. Here, the effective material property of the homogenized model shows a similar trend as that obtained using the detailed CNT model distribution.

$$E_{11} = \eta_1 V_{CNT}(z) E_{11,CNT} + V_M E_M \tag{4}$$

$$\frac{\eta_2}{E_{22}} = \frac{V_{CNT}(z)}{E_{22,CNT}} + \frac{V_M}{E_M} \tag{5}$$

$$\frac{\eta_3}{G_{12}} = \frac{V_{CNT}(z)}{G_{12,CNT}} + \frac{V_M}{G_M} \tag{6}$$

$$v_{12} = V_{CNT}^*(z) v_{12,CNT} + \left[1 - V_{CNT}(z)\right] v_M \tag{7}$$

$$\rho_{12} = V_{CNT}(z) \rho_{12,CNT} + \left[1 - V_{CNT}(z)\right] \rho_M \tag{8}$$

## 3. Numerical Example

In the numerical analysis of the natural vibration of the FG-CNTRC beam, the detailed and homogenized models are implemented using midas NFX [18], a commercial FEM program. The detailed model is analyzed three-dimensionally by creating a structure for each matrix and CNT. The homogenized model is designed to have 40 laminated plates using the composite shell element function in midas NFX. The composite shell element was developed based on the first-order shear deformation theory. The element size is set to 0.25 mm, identical to the laminated plate thickness. The length, width, and height of the homogenized model are the same as those of the detailed model. Table 4 lists the total number of elements of the detailed and homogenized models used in the analysis. The detailed model requires relatively more computation time than the homogenized model, and among the detailed models, the UD model generates the most significant number of elements. Fig. 3 shows the finite element model created using midas NFX for the detailed and homogenized models.

The detailed model of the FG-CNTRC beam and the natural frequency of the homogenized model are calculated using the mode analysis function in midas NFX. The clamped condition (CC) is applied to both ends of the beam, and the remaining boundary conditions are applied to the ends of the neutral axis of the beam. In Section 4.1, the details of the analysis on the effect of only the volume fraction on free vibration characteristics under identical simply supported (SS) boundary condition are presented. The temperature dependence of the material property is not considered in the analysis and the material properties at a temperature of 27 °C are assumed.

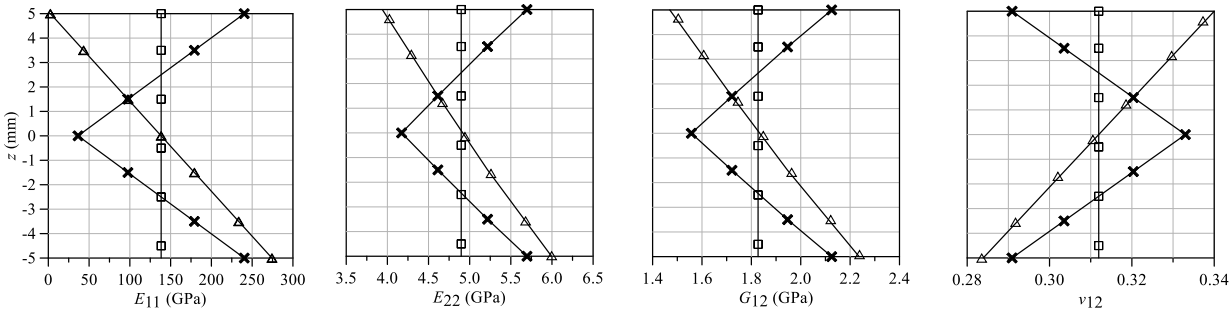


Fig. 2. Thickness-wise distributions of homogenized material properties for $V_{CNT}^{*}$ of 0.17 (□: UD, ×: FG-X, △: FG-Λ).

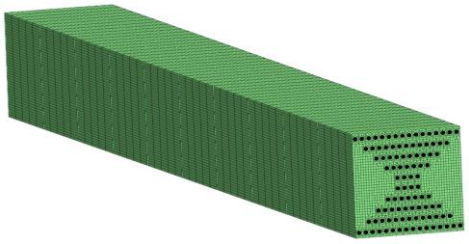

Detailed (FG-X)

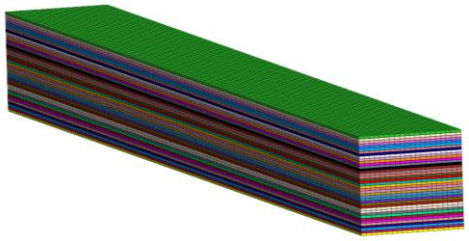

Homogenized (FG-X)

Fig. 3. Finite element models of the detailed and homogenized FG-CNTRC beams.

Table 4. Total number of elements used in FE modelling.

| $L$ (mm) | Detailed (×10$^5$) | | | Homogenized (×10$^5$) |
|---|---|---|---|---|
| | UD | FG-X | FG-Λ | |
| 100 | 1.44 | 1.22 | 1.26 | 0.16 |
| 250 | 3.60 | 3.04 | 3.16 | 0.40 |

## 4. Result and Discussion

The study compares the free vibration characteristics between the detailed and homogenized models of the FG-CNTRC beam considering changes in volume fraction and boundary conditions. All analysis results presented in this study become dimensionless upon using Eq. (9), and the relative errors $\eta_{\bar{\omega}}$ to the analytical reference solution reported in previous studies are calculated using Eq. (10).

$$\bar{\omega} = \omega L^2 \sqrt{\frac{\rho^m}{E^m h^2}} \tag{9}$$

$$\eta_{\bar{\omega}} = 100 \times \frac{\bar{\omega}_N - \bar{\omega}_A}{\bar{\omega}_A} \ (\%) , \tag{10}$$

where, $\bar{\omega}$ is the dimensionless natural frequency; $\bar{\omega}_N$ is the dimensionless natural frequency of the numerical analysis result; and $\bar{\omega}_A$ is the arithmetic mean of the analytical reference solutions.

### 4.1 Influence of Volume Fraction on the Natural Frequency

The volume fraction of the CNT is changed to 0.12, 0.17, and 0.28 to examine the free vibration characteristics of the FG-CNTRC beam according to the change in the volume fraction. To verify the reliability of the analysis results, the relative errors to the analytical reference solutions based on higher order shear deformation theory [19], Timoshenko beam theory [20], and first-order shear deformation elasticity theory [21] are calculated as in previous studies, and the results are compared. The geometric configuration of the finite element model is set to be identical to that of the model used for the analytical reference solution. Before the analysis, a convergence study was performed on the analysis error according to the element size, as shown in Fig. 4. Evidently, the element size of 2.5 mm exhibits an almost constant error level. Therefore, the free vibration analysis of UD, FG-X, and FG-Λ beams with respect to volume fraction was performed by setting the element size to 2.5 mm. Tables 5–7 list the natural frequencies of the three lower-order modes for three volume fractions.

The natural frequencies calculated via numerical analysis in this study are higher than those of the analytical reference solutions. The natural frequency increases with an increase in the volume fraction and mode of CNT. This trend is consistent with that of the typical natural vibration obtained via numerical analysis. A detailed examination of the two finite element models indicates that the relative error in the homogenized model with respect to the analytical reference solution is generally smaller than that of the detailed model. The relative error in the homogenized model ranges from 0.1 to 12.0%, whereas that of the detailed model ranges from 2.3 to 21.3%, which is a relatively wide range. This increase in error is attributed to the scale effect of the CNT structure in the detailed model. Fig. 5 schematically illustrates the average relative error of mode I to III as a function of volume fraction; the relative error is the smallest when the volume fraction is 0.17.

The relative error is high on average in the UD model and

Table 5. Comparison between the present FEA and the analytical reference solutions for various volume fractions (UD).

| $V_{CNT}^*$ | Mode | Reference solutions, $\bar{\omega}$ | | | Detailed model | | Homogenized model | |
|---|---|---|---|---|---|---|---|---|
| | | Shen and Xiang [19] | Ansari et al. [20] | Shi et al. [21] | $\bar{\omega}$ | $\eta_{\bar{\omega}}$ (%) | $\bar{\omega}$ | $\eta_{\bar{\omega}}$ (%) |
| 0.12 | Ⅰ | 15.8363 | 15.8569 | 15.8367 | 16.9684 | 7.10 | 16.2443 | 2.53 |
| | Ⅱ | 51.8139 | 51.8191 | 51.7703 | 58.8935 | 13.69 | 55.5822 | 7.30 |
| | Ⅲ | 93.8709 | 93.5513 | 93.5087 | 111.7588 | 19.34 | 104.0022 | 11.06 |
| 0.17 | Ⅰ | 19.2279 | 19.2565 | 19.2292 | 20.5790 | 6.97 | 19.3414 | 0.54 |
| | Ⅱ | 64.1381 | 64.1797 | 64.0863 | 69.1579 | 7.83 | 67.5452 | 5.32 |
| | Ⅲ | 117.8051 | 117.5724 | 117.5058 | 127.8316 | 8.67 | 128.6730 | 9.39 |
| 0.28 | Ⅰ | 23.4774 | 23.4954 | 23.4763 | 27.1594 | 15.66 | 24.2061 | 3.08 |
| | Ⅱ | 74.4687 | 74.3903 | 74.3537 | 88.4246 | 18.84 | 80.5921 | 8.32 |
| | Ⅲ | 132.2442 | 131.4391 | 131.4088 | 159.8105 | 21.35 | 147.5211 | 12.02 |

Table 6. Comparison between the present FEA and the analytical reference solutions for various volume fractions (FG-X).

| $V_{CNT}^*$ | Mode | Reference solutions, $\bar{\omega}$ | | Detailed model | | Homogenized model | |
|---|---|---|---|---|---|---|---|
| | | Shen and Xiang [19] | Ansari et al. [20] | $\bar{\omega}$ | $\eta_{\bar{\omega}}$ (%) | $\bar{\omega}$ | $\eta_{\bar{\omega}}$ (%) |
| 0.12 | Ⅰ | 18.5983 | 18.6066 | 19.2880 | 3.69 | 18.5788 | -0.13 |
| | Ⅱ | 57.5277 | 57.4088 | 64.1367 | 11.60 | 61.1982 | 6.49 |
| | Ⅲ | 100.6202 | 99.8253 | 117.5084 | 17.25 | 111.1239 | 10.88 |
| 0.17 | Ⅰ | 22.6562 | 22.7353 | 23.2266 | 2.34 | 22.5435 | -0.67 |
| | Ⅱ | 71.3956 | 71.8025 | 74.1451 | 3.56 | 75.5266 | 5.49 |
| | Ⅲ | 126.2215 | 126.6616 | 132.1270 | 4.50 | 138.9186 | 9.87 |
| 0.28 | Ⅰ | 27.1821 | 27.6011 | 30.1206 | 9.96 | 27.4551 | 0.23 |
| | Ⅱ | 80.3436 | 82.7836 | 91.4283 | 12.09 | 86.8542 | 6.49 |
| | Ⅲ | 137.3035 | 141.6530 | 158.3863 | 13.56 | 153.3781 | 9.97 |

Table 7. Comparison between the present FEA and the analytical reference solutions for various volume fractions (FG-Λ).

| $V_{CNT}^*$ | Mode | Reference solutions, $\bar{\omega}$ | | | Detailed model | | Homogenized model | |
|---|---|---|---|---|---|---|---|---|
| | | Shen and Xiang [19] | Ansari et al. [20] | Shi et al. [21] | $\bar{\omega}$ | $\eta_{\bar{\omega}}$ (%) | $\bar{\omega}$ | $\eta_{\bar{\omega}}$ (%) |
| 0.12 | Ⅰ | 13.4544 | 13.4913 | 13.4627 | 14.1796 | 5.27 | 13.6497 | 1.34 |
| | Ⅱ | 46.1920 | 46.2767 | 46.2414 | 50.1090 | 8.37 | 48.1997 | 4.25 |
| | Ⅲ | 86.8513 | 86.7826 | 86.6740 | 96.7420 | 11.49 | 92.7905 | 6.94 |
| 0.17 | Ⅰ | 16.2286 | 16.2828 | 16.2347 | 17.2131 | 5.94 | 16.4426 | 1.19 |
| | Ⅱ | 56.6836 | 56.8608 | 56.7354 | 59.0646 | 4.06 | 59.0092 | 3.96 |
| | Ⅲ | 108.1428 | 108.3287 | 108.1623 | 111.1335 | 2.70 | 115.4169 | 6.66 |
| 0.28 | Ⅰ | 19.9556 | 20.0344 | 19.9998 | 22.1701 | 10.87 | 20.6228 | 3.13 |
| | Ⅱ | 66.9973 | 67.4387 | 67.3595 | 75.8892 | 12.82 | 71.9576 | 6.98 |
| | Ⅲ | 123.8009 | 124.5196 | 124.4277 | 145.3869 | 17.01 | 136.9897 | 10.25 |

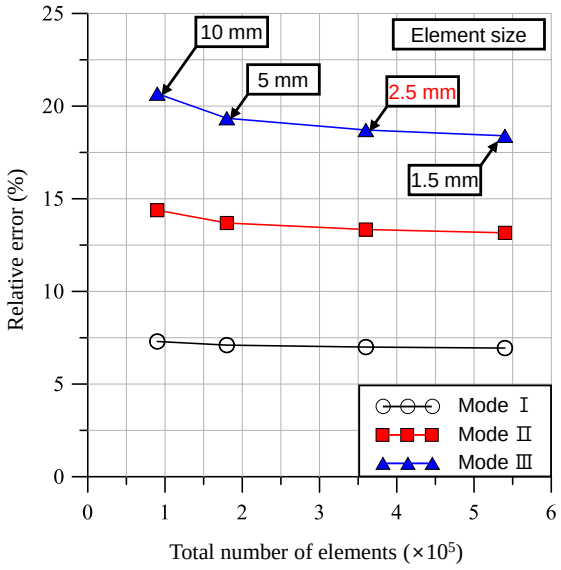


Fig. 4. Variation of the relative error of the three lowest natural frequencies to the element size ( $V_{CNT}^{*}$ = 0.12).

relatively low in the FG-X and FG-Λ models, as determined by the free vibration characteristics according to the type of functional gradient. By contrast, the relative error based on the type of functional gradient in the detailed model is also more significant than that of the homogenized model. The range of the relative error based on the volume fraction change is significantly higher in the detailed model than that in the homogenized model.

Consequently, the natural frequencies of the detailed and homogenized models yield a relative error of approximately 20% based on the volume fraction compared to that of the analytical reference solution. However, the absolute value of the relative error in the homogenized model is smaller than that of the detailed model. The difference in the relative error according to the change in volume fraction and the type of functional gradient is also minor.

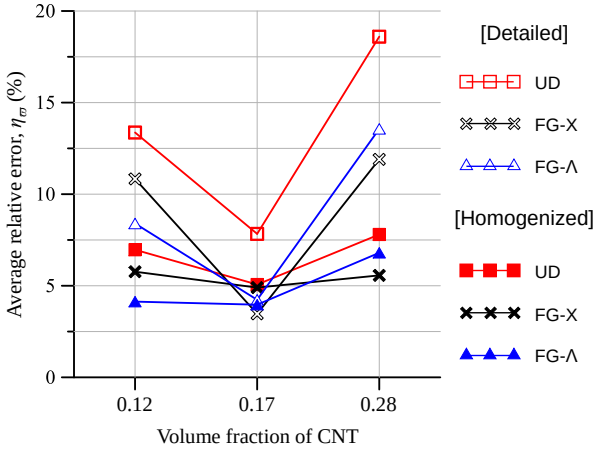


Fig. 5. The average relative errors versus the volume fractions.

## 4.2 Influence of Boundary Condition on the Natural Frequency

Understanding the free vibration characteristics for various boundary conditions is crucial because the FG-CNTRC beam can be used in multiple applications. Therefore, the CNT volume fraction was set to 0.12 in this study and the eigen behavior of the detailed and homogenized models under various boundary conditions was compared. The length of the beam was set to 100 mm for an evaluation equivalent to the geometric conditions used to obtain the analytical reference solution, and the element size was set as 2.5 mm according to the convergence study presented in Section 4.1; SS, CC, and FF were selected as boundary conditions, and the analysis results are listed in Tables 8 – 10.

The relative errors of both the detailed and homogenized models increased significantly compared to the analytical reference solution discussed in Section 4.1, which can be explained by the change in the length of the target model, considering that the relative error also increased in the SS boundary condition of the previous analysis. However, as the natural frequency increased, the relative error also increased as a function of the natural frequency, but the characteristic of the homogenized model yielding lower relative error than the detailed model remained unchanged. Quantitatively speaking, the relative error of the homogenized model was in the range of 0.4 – 20.1%, whereas that of the detailed model ranged between 3.5 – 39.3%, showing an error of up to 40%. It is observed that a relatively high error rate occurs if the nanomaterial size is increased, as in the detailed model. Fig. 6 shows the three low-order mode shapes calculated by the detailed and homogenized models. The mode shapes of CNT in the detailed model are displayed separately for reference.

Comparing the free vibration characteristics according to the type of functional gradient, it is observed that the relative error of both the detailed model and the homogenized model is the largest in the UD model and the smallest in the FG-Λ model. The significance of the relative errors is in the order of CC, FF, and SS in terms of the boundary condition. Fig. 7 shows the average relative error of the three low-order modes according to the boundary condition. Evidently, the homogenized model has a significantly lower average relative error than that of the detailed model, and the FG-Λ model shows significantly lower relative error than those of the UD and FG-X models. Consequently, the free vibration characteristics of both the detailed model and the homogenized model change according to the functional gradient type and the boundary condition, similar to the analytical reference solution of previous studies. However, the homogenized model yields a relative error of approximately 20%, whereas the detailed model yields a relative error of approximately 40%.

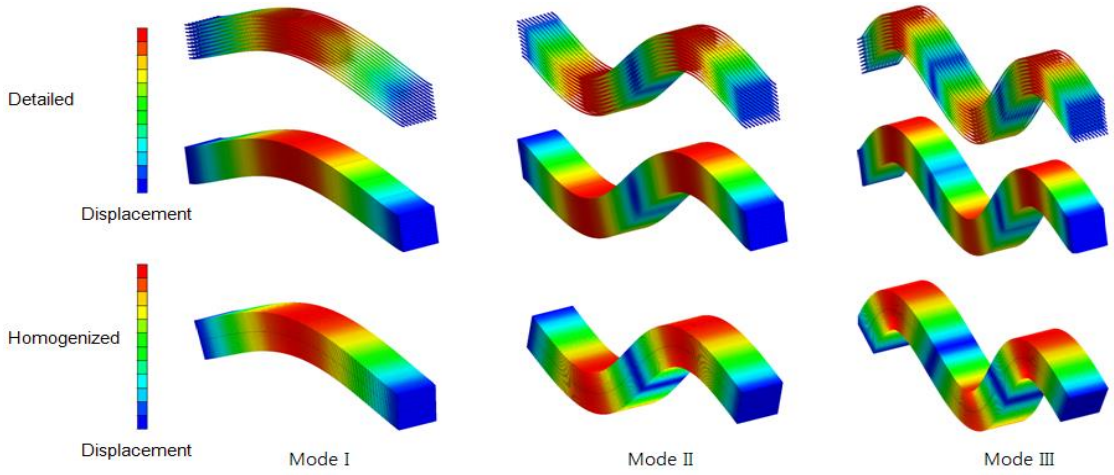


Fig. 6. Three lowest vertical bending mode shapes of UD CNTRC beam under clamped-clamped condition ($L$ = 100 mm, $V_{CNT}^{*}$ = 0.12).

Table 8. Comparison between the present FEA and the analytical reference solutions for different boundary conditions (UD).

| Boundary condition | Vertical bending mode | Reference solutions, $\bar{\omega}$ | Detailed model | | Homogenized model | |
|---|---|---|---|---|---|---|
| | | Shi et al. [20] | $\bar{\omega}$ | $\eta_{\bar{\omega}}$ (%) | $\bar{\omega}$ | $\eta_{\bar{\omega}}$ (%) |
| SS | Ⅰ | 11.3232 | 13.5517 | 19.68 | 12.6801 | 11.98 |
| | Ⅱ | 27.9037 | 35.1221 | 25.87 | 32.8054 | 17.57 |
| | Ⅲ | 44.0270 | 57.1730 | 29.86 | 52.6087 | 19.49 |
| CC | Ⅰ | 14.2538 | 19.0275 | 33.49 | 16.8705 | 18.36 |
| | Ⅱ | 28.5113 | 39.0105 | 36.82 | 33.9440 | 19.05 |
| | Ⅲ | 44.3037 | 61.7196 | 39.31 | 53.1105 | 19.88 |
| FF | Ⅰ | 23.9206 | 29.0976 | 21.64 | 27.0334 | 13.01 |
| | Ⅱ | 40.3698 | 52.8469 | 30.91 | 47.6675 | 18.08 |
| | Ⅲ | 57.7140 | 77.6325 | 34.51 | 68.7959 | 19.20 |

Table 9. Comparison between the present FEA and the analytical reference solutions for different boundary conditions (FG-X).

| Boundary condition | Vertical bending mode | Reference solutions, $\bar{\omega}$ | Detailed model | | Homogenized model | |
|---|---|---|---|---|---|---|
| | | Shi et al. [20] | $\bar{\omega}$ | $\eta_{\bar{\omega}}$ (%) | $\bar{\omega}$ | $\eta_{\bar{\omega}}$ (%) |
| SS | Ⅰ | 12.3011 | 14.2257 | 15.65 | 13.7337 | 11.65 |
| | Ⅱ | 28.8111 | 35.4288 | 22.97 | 33.9625 | 17.88 |
| | Ⅲ | 44.7878 | 56.4980 | 26.15 | 53.6449 | 19.78 |
| CC | Ⅰ | 14.6267 | 19.3683 | 32.42 | 17.3575 | 18.67 |
| | Ⅱ | 29.1546 | 39.3746 | 35.05 | 34.7298 | 19.12 |
| | Ⅲ | 44.9606 | 61.8338 | 37.53 | 53.9928 | 20.09 |
| FF | Ⅰ | 25.7045 | 31.0486 | 20.79 | 29.0337 | 12.95 |
| | Ⅱ | 41.5025 | 53.9036 | 29.88 | 49.1524 | 18.43 |
| | Ⅲ | 58.8994 | 78.3622 | 33.04 | 70.3140 | 19.38 |

Table 10. Comparison between the present FEA and the analytical reference solutions for different boundary conditions (FG-Λ).

| Boundary condition | Vertical bending mode | Reference solutions, $\bar{\omega}$ | Detailed model | | Homogenized model | |
|---|---|---|---|---|---|---|
| | | Shi et al. [20] | $\bar{\omega}$ | $\eta_{\bar{\omega}}$ (%) | $\bar{\omega}$ | $\eta_{\bar{\omega}}$ (%) |
| SS | Ⅰ | 11.1214 | 11.5080 | 3.48 | 11.1649 | 0.39 |
| | Ⅱ | 26.8855 | 31.1999 | 16.05 | 30.2861 | 12.65 |
| | Ⅲ | 43.3760 | 51.3902 | 18.48 | 49.4608 | 14.03 |
| CC | Ⅰ | 13.8550 | 17.0917 | 23.36 | 15.6939 | 13.27 |
| | Ⅱ | 27.9120 | 35.3938 | 26.80 | 31.8359 | 14.06 |
| | Ⅲ | 43.7355 | 56.3146 | 28.76 | 50.1487 | 14.66 |
| FF | Ⅰ | 21.9745 | 25.0642 | 14.06 | 23.9530 | 9.00 |
| | Ⅱ | 39.1137 | 46.9762 | 20.10 | 44.1884 | 12.97 |
| | Ⅲ | 56.5360 | 69.5204 | 22.97 | 64.4742 | 14.04 |

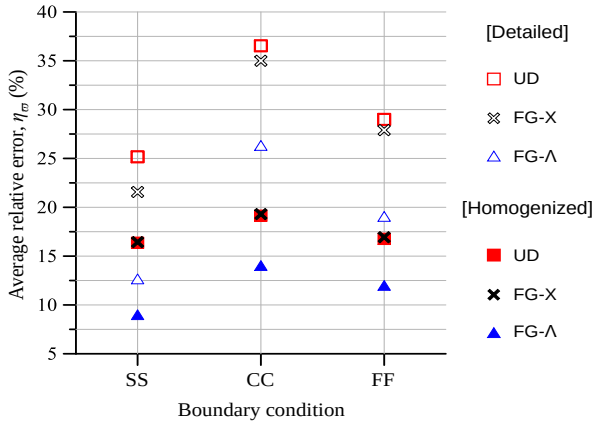


Fig. 7. The average relative errors for different boundary conditions.

### 4.3 Characteristics of the Higher-order Natural Modes

Next, the characteristics of higher-order natural models obtained using the detailed and homogenized models are investigated. The same geometry and dimensions are used and the CNT volume fraction $V_{CNT}^{*}$ is taken by 0.12. Table 11 compares 9 lowest natural modes of the detailed and homogenized models for UD, FG-X and FG-Λ CNTRC beams. First of all, three different natural modes, the vertical and lateral bending modes and the twisting modes are come out. The order in the appearance of these modes is influenced by the FEM model, the CNT distribution type and the boundary condition, except for the FF condition where the appearing order is T→VB→LB. In the SS and CC conditions, the appearing order is either LB→VB→T or VB→LB→T depending on the FEM model and the CNT distribution type. Figs. 9 and 10 represent three lowest lateral bending modes and three lowest twisting modes of UD CNTRC beam under the clamped-clamped condition, respectively.

## 5. Conclusion

This study compared the free vibration characteristics of the detailed model with those of the homogenized model for the FG-CNTRC beam and analyzed the effect of the volume fraction distribution and the boundary condition type. A 3-D FEA was performed using the detailed model by implementing an enlarged CNT structure. For the homogenized model, the effective material properties were calculated, and a 2-D FEA was performed for a laminated plate using a composite shell element. The analysis results of the detailed and homogenized models obtained through FEA were compared with the analytical reference solutions reported in previous studies.

The main conclusions obtained from the analysis results are as follows.

- The homogenized model shows a relatively small relative error compared to the analytical reference solutions.
- The natural frequency of the FG-CNTRC beam increases as the CNT volume fraction increases, and the average relative error to the analytical reference solution is the smallest when the volume fraction is 0.17.
- The UD model yields a higher relative error to the analytical reference solution than that of other functional gradient types under the same conditions, and the FG-Λ model yields the lowest relative error on average.
- The boundary condition, on average, yields the highest relative error for the CC condition and the lowest for the SS condition compared to the analytical reference solution.
- The detailed model is less suitable in practice if the analytical reference solution presented herein is assumed to the actual value. By contrast, a homogenized model with an approximately 5% average relative error is suitable for practical use.

The proposed FEM models suffer from the mesh-dependent numerical error and cannot account for the nonlinear free vibration. But, the proposed models can deal with the practical beam-like structures having more complicated geometry and CNT

distribution than the analytical reference models.

Table 11. Comparison of bending and twisting modes between the detailed and homogenized models for three boundary conditions ( $V_{CNT}^{*}$ =0.12).

| Boundary condition | Mode | UD | | FG-X | | FG-Λ | |
|---|---|---|---|---|---|---|---|
| | | Detailed | Homogenized | Detailed | Homogenized | Detailed | Homogenized |
| SS | 1 | 13.2327 (LB1) | 12.6801 (VB1) | 11.2917 (LB1) | 13.7337 (VB1) | 11.5080 (VB1) | 11.1649 (VB1) |
| | 2 | 13.5517 (VB1) | 17.2225 (LB1) | 14.2257 (VB1) | 17.2457 (LB1) | 12.0126 (LB1) | 16.3898 (LB1) |
| | 3 | 19.3355 (T1) | 18.7243 (T1) | 18.0612 (T1) | 19.0227 (T1) | 18.2678 (T1) | 18.6100 (T1) |
| | 4 | 33.0087 (LB2) | 32.8054 (VB2) | 29.2446 (LB2) | 33.9625 (VB2) | 28.4052 (LB2) | 30.2861 (VB2) |
| | 5 | 35.1221 (VB2) | 34.9674 (LB2) | 35.4288 (VB2) | 35.0173 (LB2) | 31.1999 (VB2) | 33.5891 (LB2) |
| | 6 | 39.0256 (T2) | 37.6153 (T2) | 36.4354 (T2) | 38.2572 (T2) | 38.0920 (T2) | 37.4406 (T2) |
| | 7 | 52.9775 (LB3) | 52.6087 (VB3) | 47.4195 (LB3) | 53.6449 (VB3) | 45.2803 (LB3) | 49.4608 (VB3) |
| | 8 | 57.1730 (VB3) | 55.0001 (LB3) | 55.4867 (T3) | 55.0824 (LB3) | 51.3902 (VB3) | 52.6823 (LB3) |
| | 9 | 59.2634 (T3) | 56.7006 (T3) | 56.4980 (VB3) | 57.7093 (T3) | 59.3479 (T3) | 57.0555 (T3) |
| CC | 1 | 19.0275 (VB1) | 16.8705 (VB1) | 17.2048 (LB1) | 17.2457 (LB1) | 16.0766 (LB1) | 15.6939 (VB1) |
| | 2 | 19.0276 (LB1) | 17.2225 (LB1) | 19.3683 (VB1) | 17.3575 (VB1) | 17.0917 (VB1) | 16.7583 (LB1) |
| | 3 | 22.2515 (T1) | 18.9019 (T1) | 22.0301 (T1) | 19.2291 (T1) | 22.2322 (T1) | 1 8.7150 (T1) |
| | 4 | 39.0105 (VB2) | 33.9440 (VB2) | 35.8616 (VB2) | 34.7298 (VB2) | 33.5392 (LB2) | 31.8359 (VB2) |
| | 5 | 39.0107 (LB2) | 34.9674 (LB2) | 39.3746 (LB2) | 35.0173 (LB2) | 35.3938 (VB2) | 34.0964 (LB2) |
| | 6 | 44.7340(T2) | 37.8790 (T2) | 44.2778 (T2) | 38.5424 (T2) | 44.9245 (T2) | 37.5893 (T2) |
| | 7 | 61.7196 (VB3) | 53.1105 (VB3) | 57.2971 (LB3) | 53.9928 (VB3) | 53.0285 (LB3) | 50.1487 (VB3) |
| | 8 | 67.6118 (LB3) | 55.0001 (LB3) | 61.8338 (VB3) | 55.0824 (LB3) | 56.3146 (VB3) | 53.1151 (LB3) |
| | 9 | 84.8562 (T3) | 56.9759 (T3) | 66.9065 (T3) | 57.9901 (T3) | 68.5600 (T3) | 57.1700 (T3) |
| FF | 1 | 21.5069 (T1) | 18.7113 (T1) | 21.2901 (T1) | 19.0027 (T1) | 20.9796 (T1) | 18.3075 (T1) |
| | 2 | 29.0976 (VB1) | 27.1792 (VB1) | 24.6627 (LB1) | 27.2025 (LB1) | 23.2298 (LB1) | 23.9530 (VB1) |
| | 3 | 29.0978 (LB1) | 27.1792 (LB1) | 31.0486 (VB1) | 29.0337 (VB1) | 25.0642 (VB1) | 26.5666 (LB1) |
| | 4 | 43.2903 (T2) | 37.5443 (T2) | 42.8669 (T2) | 38.1601 (T2) | 42.5393 (T2) | 36.8369 (T2) |
| | 5 | 52.8469 (LVB2) | 47.6675 (VB2) | 47.3108 (LB2) | 48.4927 (LB2) | 44.1251 (LB2) | 44.1884 (VB2) |
| | 6 | 52.8473 (LB2) | 48.4288 (LB2) | 53.9036 (VB2) | 49.1524 (VB2) | 46.9762 (VB2) | 47.2390 (LB2) |
| | 7 | 65.5190 (T3) | 56.5534 (T3) | 64.8602 (T3) | 57.5260 (T3) | 64.8691 (T3) | 55.7022 (T3) |
| | 8 | 77.6325 (VB3) | 68.7959 (VB2) | 70.6295 (LB3) | 70.3140 (VB3) | 65.2771 (LB3) | 64.4742 (VB3) |
| | 9 | 77.6330 (LB3) | 70.6160 (LB2) | 78.3622 (VB3) | 70.7167 (LB3) | 69.5204 (VB3) | 68.6145 (LB3) |

* VB: vertical bending mode, LB: lateral bending mode, T: twisting mode

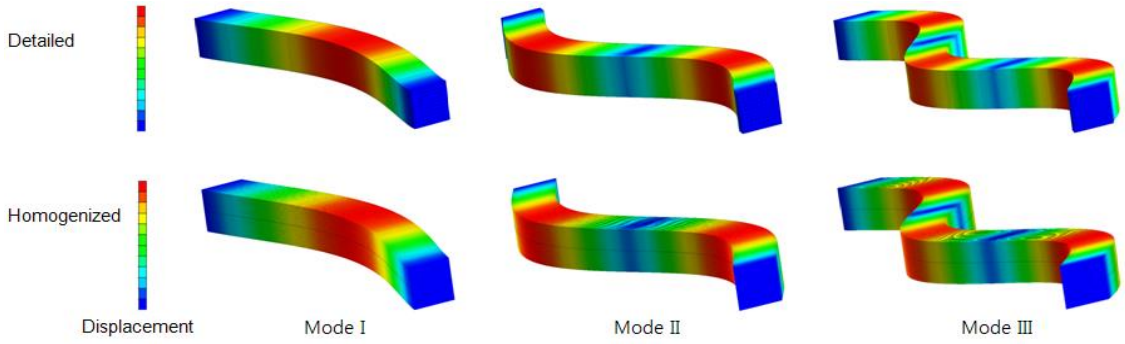


Fig. 8. Three lowest lateral bending mode shapes of UD CNTRC beam under clamped-clamped condition ($L$ = 100 mm, $V_{CNT}^{*}$ = 0.12).

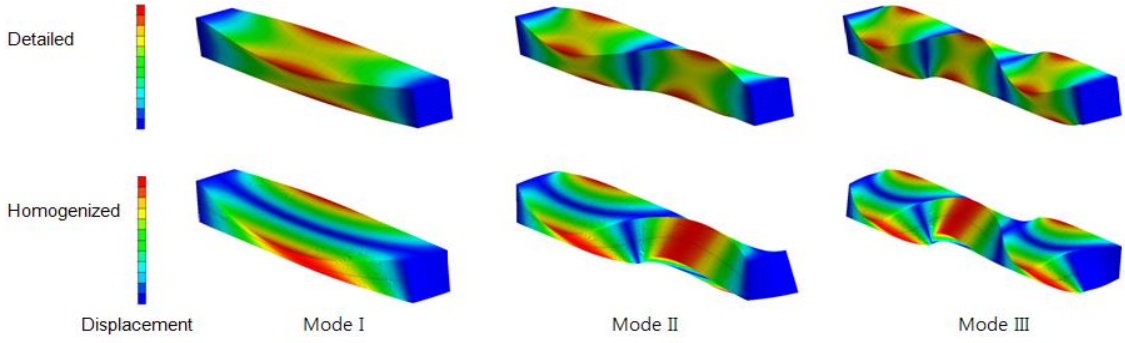


Fig. 9. Three lowest twisting mode shapes of UD CNTRC beam under clamped-clamped condition ($L$ = 100 mm, $V_{CNT}^{*}$ = 0.12).

## Acknowledgments

This work was supported by the National Research Foundation of Korea (NRF) grant funded by the Korea government (MSIT) (No.2020R1A2C110029).

## References

[1] N.D. Duc, Nonlinear Static and Dynamic Stability of Functionally Graded Plates and Shells, Vietnam National University Press, Hanoi (2014).
[2] J.N. Reddy, Microstructure-dependent couple stress theories of functionally graded beams, Journal of the Mechanics and Physics of Solids, 59 (2011) 2382-2399.
[3] M.H. Yas and N. Samadi, Free vibrations and buckling analysis of carbon nanotube-reinforced composite Timoshenko beams on elastic foundation, International Journal of Pressure Vessels and Piping, 98 (2012) 119-128.
[4] Ghorbani Shenas A., Malekzadeh P., and Ziaee S., Vibration analysis of pre-twisted functionally graded carbon nanotube reinforced composite beams in thermal environment, Composite Structures, 162 (2017) 325-340.
[5] N.D. Duc, T.Q. Quan, N.D. Khoa, New approach to investigate nonlinear dynamic response and vibration of imperfect functionally graded carbon nanotube reinforced somposite double curved shallow shells subjected to blast load and temperature, Aerospace Science and Technology, 71 (2017) 360-372.
[6] N.D. Duc, P.P. Minh, Free vibration analysis of cracked FG CNTRC plates using phase field theory, Aerospace Science and Technology, 112 (2021) 106654.
[7] N.V. Thanh, N.D. Khoa, ND Tuan, P. Tran, N.D. Duc, Nonlinear dynamic response and vibration of functionally graded carbon-reinforced composite 9FG-CNTRC0 shear deformable plates with temperature-dependent material properties and surrounded on elastic foundations, Journal of Thermal Stressess, 40(1) (2017) 1254-1274.
[8] Karamanli A. and Vo T.P., Finite element model for carbon nanotube-reinforced and graphene nanoplatelet-reinforced composite beams, Composite Structures, 264 (2021) 113739.
[9] N.D. Dat, N.V. Thanh, V.M. Anh, N.D. Duc, Vibration and nonlinear dynamic analysis of sandwich FG-CNTEC plate with porous core layer, Mechanics of Advanced Materials and Structures, 29(10) (2022) 1431-1448.
[10] J.R. Cho, Free vibration analysis of functionally graded sandwich plates with a homogeneous core, Applied Aciences, 12 (2022) 6054.
[11] S. Yang, S. Yu and M. Cho, A study on the development of multiscale bridging method consideringthe particle size and concentration effect of nanocomposites, Journal of the Computational Structural Engineering Institute of Korea, 22 (4) (2009) 343-348.
[12] H.S. Shen and C.L. Zhang, Thermal buckling and postbuckling behavior of functionally graded carbon nanotube-reinforced composite plates, Materials & Design, 31 (7) (2010) 3403-3411.
[13] J.R. Cho and J.T. Oden, Functionally graded material: a parametric study on thermal-stress characteristics using the Crank–Nicolson–Galerkin scheme, Computer Methods in Applied Mechanics and Engineering, 188 (1-3) (2000) 17-38.
[14] J.R. Cho and D.Y. Ha, Averaging and finite-element discretizing approaches in the numerical analysis of functionally graded materials, Materials Science and Engineering A, 302 (2001) 187-196.
[15] T. Mori and K. Tanaka, Average stress in matrix and average elastic energy of materials with misfitting inclusions, Acta metallurgica, 21 (5) (1973) 571-574.
[16] R. Hill, A self-consistent mechanics of composite materials, Journal of the Mechanics and Physics of Solids, 13 (4) (1965) 213-222.
[17] K.S. Ravichandran, Elastic properties of two-phase composites, Journal of the American Ceramic Society, 77 (5) (1994) 1178-1184.
[18] MIDAS, Analysis manual - midas NFX, Modelling, Integrated Design and Analysis Software, Gyeonggi-do, South Korea (2020).
[19] H.-S. Shen and Y. Xiang, Nonlinear analysis of nanotube-reinforced composite beams resting on elastic foundations in thermal environments, Engineering Structures, 56 (2013) 698-708.
[20] R. Ansari, M. Faghih Shojaei, V. Mohammadi, R. Gholami, and F. Sadeghi, Nonlinear forced vibration analysis of functionally graded carbon nanotube-reinforced composite Timoshenko beams, Composite Structures, 113 (2014) 316-327.
[21] Z. Shi, X. Yao, F. Pang, and Q. Wang, An exact solution for the free-vibration analysis of functionally graded carbon-nanotube-reinforced composite beams with arbitrary boundary conditions, Scientific Reports, 7 (2017) 12909.

## Author information

**Hyeong Jin Kim** received his B.S. and M.S. degree from the Hongik University and Pusan National University in 2020 and 2022, respectively. He is currently a Ph.D. student at the department of Mechanical Engineering in University College London. His major research field is the nonlinear structural mechanics, analysis, and design of ships and offshore structures.

**Jin-Rae Cho** received his B.S. degree in Aeronautical Engineering from Seoul National University in 1983. He then received his M.S. and Ph.D. degrees from the University of Texas at Austin in 1993 and 1995, respectively. He is currently a Professor at the Department of Naval Architecture and Ocean Engineering in Hongik University. His major research field is the computational mechanics in solid/structural mechanics, ocean engineering and materials science.